Energy and AI 16 (2024) 100340

Contents lists available at ScienceDirect

Energy and AI

journal homepage: www.elsevier.com/locate/egyai

# Distributed scheduling for multi-energy synergy system considering renewable energy generations and plug-in electric vehicles: A level-based coupled optimization method

Linxin Zhang [a,b], Zhile Yang [b,*], Qinge Xiao [b], Yuanjun Guo [b], Zuobin Ying [a], Tianyu Hu [b], Xiandong Xu [c], Sohail Khan [e], Kang Li [d]

[a] Faculty of Data Science, City University of Macau, Taipa, 999078, Macau
[b] Shenzhen Institute of Advanced Technology, Chinese Academy of Sciences, Shenzhen, Guangdong, 518055, China
[c] Tianjin University, Tianjin 300072, China
[d] School of Electronic and Electrical Engineering, University of Leeds, Leeds, LS2 9JT, UK
[e] Institute of Applied Sciences & Technology, Pak-Austria Fachhochschule, Haripur, Khyber Pakhtunkhwa, Pakistan

## HIGHLIGHTS

- Design of a novel multi-energy synergy system scheduling framework.
- Costs of power generation and carbon emissions of the units and plug-in electric vehicles are considered.
- Binary level-based learning swarm optimizer is proposed for solving strongly coupled unit commitment problems.
- Charging and discharging management of electric vehicles, energy and economic benefits are obtained.
- Effects of three different scenarios into the power system are comparatively studied.

## GRAPHICAL ABSTRACT

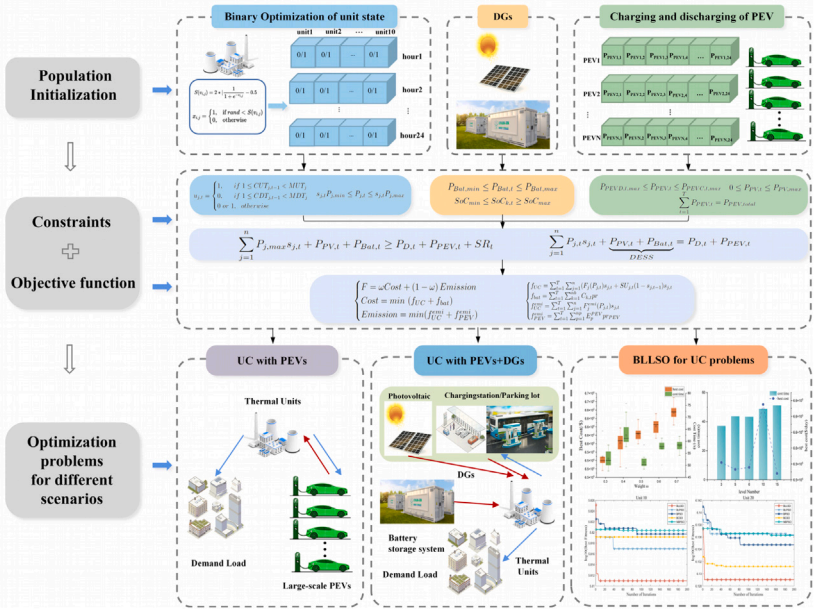


## ARTICLE INFO

*Keywords:*
Electric vehicle
Unit commitment
Renewable energy

## ABSTRACT

Multi-energy synergy systems integrating high-penetration large-scale plug-in electric vehicles, distributed renewable energy generations, and battery energy storage systems have great potential to reduce the reliance of the grid on traditional fossil fuels. However, the random charging characteristics of plug-in electric vehicles

* Corresponding author.
*E-mail addresses:* lx.zhang1@siat.ac.cn (L. Zhang), zyang07@qub.ac.uk (Z. Yang), qg.xiao@siat.ac.cn (Q. Xiao), yj.guo@siat.ac.cn (Y. Guo), ty.hu@siat.ac.cn (T. Hu), xux27@tju.edu.cn (X. Xu), sohail.khan@gmx.net (S. Khan), k.li1@leeds.ac.uk (K. Li).

https://doi.org/10.1016/j.egyai.2024.100340
Received 7 November 2023; Received in revised form 30 December 2023; Accepted 15 January 2024
Available online 20 January 2024

Battery energy storage system
Synergy optimization

and the uncertainty of photovoltaics may impose an additional burden on the grid and affect the supply–demand equilibrium. To address this issue, judicious scheduling optimization offers an effective solution. In this study, considering charge and discharge management of plug-in electric vehicles and intermittent photovoltaics, a novel Multi-energy synergy systems scheduling framework is developed for solving grid instability and unreliability issues. This formulates a large-scale mixed-integer problem, which calls for a powerful and effective optimizer. The new binary level-based learning optimization algorithm is proposed to address nonlinear large-scale high-coupling unit commitment problems. To investigate the feasibility of the proposed scheme, numerical experiments have been carried out considering multiple scales of unit numbers and various scenarios. Finally, the results confirm that the proposed scheduling framework is reasonable and effective in solving unit commitment problems, can achieve 3.3% cost reduction and demonstrates superior performance in handling large-scale energy optimization problems. The integration of plug-in electric vehicles, distributed renewable energy generations, and battery energy storage systems is verified to reduce the output power of 192.72 MW units during peak periods to improve grid stability. Therefore, optimizing energy utilization and distribution will become an indispensable part of future power systems.

## 1. Introduction

The primary strategy in the energy sector for reducing carbon emissions has consistently been the global transition to multi-energy decarbonization, which involves replacing conventional power generation methods with renewable energy sources [1]. Due to the imbalance of energy resource distributions [2], major countries, such as China, are heavily relying on coal-fired power plants for heating and power supply [3]. The Multi-Energy Synergy System (MESS) seamlessly integrates plug-in electric vehicles (PEV) [4], distributed renewable energy generations (DRGs) [5] like photovoltaic, and battery energy storage systems (BESS) [6] into conventional thermal power units. This integrated framework harmoniously amalgamates various energy types, leveraging intelligent optimization technologies to efficiently manage energy transmission, storage, power generation, and consumption [7], fostering collaborative operation among different system components. Different from Integrated Energy Systems (IES), MESSs place a greater emphasis on cultivating deeper synergies and interactions among diverse energy sources. The technical design of MESSs is characterized by its enhanced flexibility, enabling swift adaptation actively to fluctuations in power demand and energy supply. This adaptability proves instrumental in effectively managing the variability and peak load demands associated with DRGs.

The large-scale incorporation of multiple energy sources within the MESSs introduces a significant challenge of pronounced energy volatility, which can lead to power grid instability. Consequently, the generating units within the MESSs are compelled to engage in frequent start and stop operations to uphold energy equilibrium, thereby exacerbating the economic burden [8], which is typically referred to as the unit commitment (UC) problem. Currently, the integration of the PEVs, DRGs, and BESS modules into the power system, respectively, along with their rational scheduling optimization, has become a viable approach to addressing UC problems. Firstly, submodule PEVs in MESSs can alleviate the load burden on the power grid by avoiding the overload phenomenon of the grid during the peak period [9] and implementing intelligent scheduling of the charge and discharge management [10]. In [11], a constrained optimization approach was proposed to accomplish cost-conscious battery charging from PEV users. Secondly, DRGs integrated into MESSs [12], such as photovoltaics [13], may help alleviate the burden on the electrical system [14]. In [15], a stochastic programming scheduling model was proposed to minimize the prediction error of photovoltaic, which can improve voltage stability of power systems. However, current conventional systems still rely on non-renewable [16], readily available reserves in order to maintain a stable supply of on-demand energy and minimize generation during times of excess energy production [17]. In [18,19], they addressed the traditional combinatorial optimization problems to manage the coordinated and uncoordinated charging system of grid-connected EVs with photovoltaic. Thirdly, similar to DRGs and PEVs, coordinated BESS in MESSs also brings numerous benefits to the power grid system [20], such as reducing operation costs [21], voltage control [22] and operating as a reserve of the electrical grid [23]. BESS for MESSs has been proven to be an efficient means to ensure the efficient, dependable, and real-time functioning of modern power grids [24]. In [25], a distributed battery system was proposed to propose a distributed battery system to reduce required battery capacities through enhanced excess sharing and storage sharing.

The above research lays a strong foundation on the cutting edge. The coupling relationship between DRGs, PEVs and BESS within MESSs creates a coordinated energy ecosystem that promotes the utilization of renewable resources and enhances the flexibility and reliability of the grid. Nonetheless, on account of the intermittent nature of the majority of DRGs, PV is susceptible to weather conditions [26], the turbulence of the power system will become more distinct in the future as the ever-growing proportion of DRGs in the power supply structure [27]. Additionally, the installation cost of BESS is considerably high, and several BESSs entail additional maintenance expenses [28]. Simultaneously, the unpredictable charging patterns of large-scale PEVs pose inherent challenges to the reliability [29] and security [30] of the power grid. With the large-scale popularization and application of electric vehicles and DRGs [31], the data complexity grows, necessitating increased inter-module coupling for the MESSs.

For traditional power grid systems that only consider the integration of PEVs, DRGs or BESS, this is a typical nonlinear mixed integer optimization problem. Conventional approaches utilized to address this type of scheduling optimization problems are broadly classified into the mathematical methods and the meta-heuristic algorithms (MAs). Widely used mathematical methods such as stochastic mixed-integer programming [32], parallel dual dynamic integer programming [33], Lagrange relaxation [34] and Quantum Surrogate Lagrangian Relaxation (QSLR) [35] were easy to implement with low-dimensional UC problems. Different from the mathematical approaches, conventional MA methods, such as genetic algorithm (GA) [36], differential evolution (DE) [37], ant colony optimization (ACO) [38], particle swarm optimization (PSO) [39], firefly algorithm [40] and teaching learning based optimization (TLBO) [41]. Because of flexible encoding techniques and superior optimization processes, MAs can obtain better outcomes when tackling UC optimization problems. In addition, several binary-coded variants of MAs have been proposed to address UC binary conversion problems, where the start–stop state decision variable of the generating unit is binary. Binary differential evolution (BDE) [42], binary particle swarm optimization (BPSO) [8], binary whale optimization algorithm (BWOA) [43], binary fish migration optimization [44] and binary artificial bee colony (DisABC) [45] methods utilized transfer functions to map the search space. While quantum-inspired particle swarm optimization (QPSO) [46] and quantum-based sine cosine algorithm (Q-SCA) [47] combined with quantum computing to improve search ability, as well as some mixed binary code schemes such as mixed-variable version PSO [48] and etc. Through base conversion, the binary MA methods can effectively address mixed-integer problems, showcasing significant potential for handling large-scale MESSs

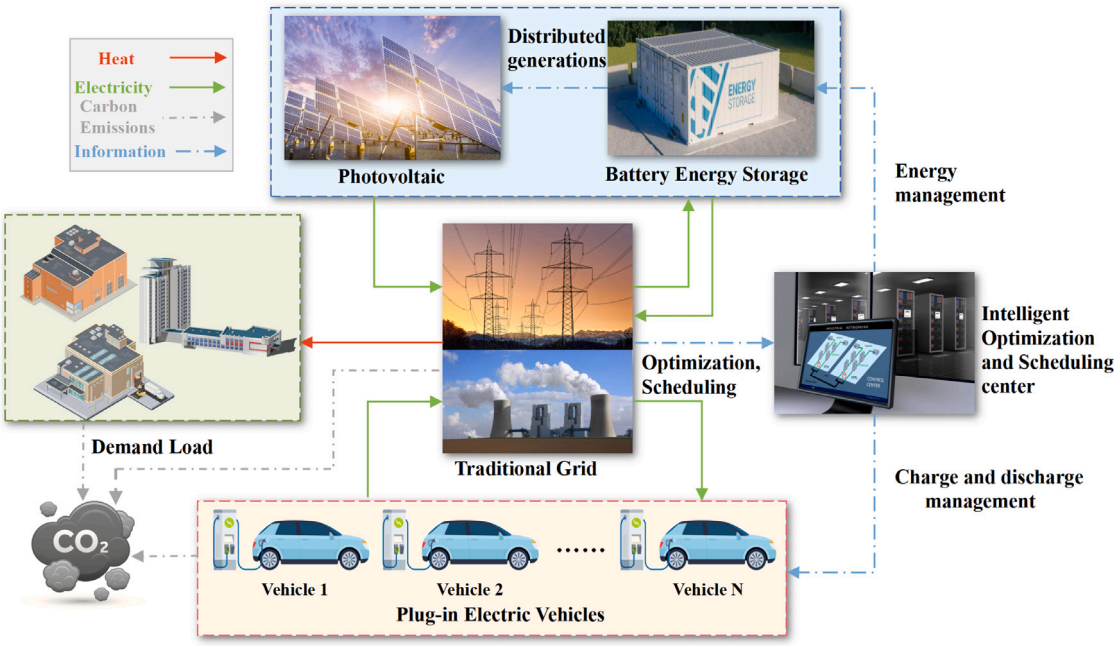


**Fig. 1.** Architecture of MESSs.

integration. As system complexity increases, some novel learning strategies for PSO were developed to improve algorithm performance. The competitive learning strategy [49], mutation-PSO [50] and the social learning strategy [51] inspired by competition and cognition in human society. The tricompetition mechanism [52] was applied for CSO to reduce the sparsity of optimal solutions. Subsequently, BCSO [53] and BSLPSO [54] utilized the mechanism that the superior particles in the present swarm to facilitate the update of other particles so that enhanced the diversity of the population. Due to the synergy between different energy flows, MESS optimization becomes a large-scale strongly coupled mixed integer optimization problem. In [55], a multispace evolutionary search was proposed to divide up the large-scale problem into multiple subproblems. The fast-forward selection-based heuristic algorithm was designed in [56] to facilitate the decomposition of large-scale problems. Unlike BCSO and BSLPSO which only use the position of the one better particle to update the positions of other particles at each iteration, the level-based learning swarm optimizer (LLSO) [57] divided different particles into different levels and each particle in each level could update its position according to two better particles from two randomly selected levels. This strategy not only improves diversity, but also balances exploration and exploitation.

Based on the aforementioned research, this paper introduces a multi-energy synergy optimization framework to minimize generation cost of system components, start–stop costs of units and $CO_2$ emission costs. The level-based learning strategy is applied for the MESS optimization design to evaluate the influence of incorporating BESS and PV as distributed generations (DGs), along with the charge and discharge management of large-scale PEVs within the power system. Moreover, a binary level-based learning swarm optimization algorithm is developed in this paper to tackle the binary decision variable encoding problem in EMS optimization. In this end, three different scenarios have been performed to validate the feasibility and effectiveness of proposed MESS scheduling framework. To the best of our knowledge, this MESS is the first proposed for tackling high dimension combinatorial optimization problems. Several significant contributions of this research are highlighted as follows:

- A highly integrated MESS scheduling is developed for the first time to expand from a single energy source to multi-energy integration of PEVs, DRGs and BESS, considering dynamic real-time multi-energy management and optimization.
- A high-coupling and nonlinear model is formulated, to minimize power generation costs and carbon emissions under system-wide and unit-wise constraints.
- A novel binary level-based learning swarm algorithm is proposed to prevent the curse of dimensionality and binary variables transfer when tackling the large scale MESS optimization problem by enhancing the population diversity.

The following sections of this paper are arranged as follows: the MESS problem formulation taking account into DGs and PEVs is given by Section 2. Section 3 presents the proposed MESSs scheduling framework as well as a full process illustration of the proposed BLLSO optimization approach. Section 4 shows the experimental results and provides an in-depth analysis of the findings. The paper's description of the main ideas is concluded by Section 5.

## 2. Problem formulation

In this section, the architecture of the proposed MESSs is illustrated firstly. To optimize the economic cost of the thermal units and reduce carbon emissions, the carbon emission and fossil fuel costs are regarded as the objective function in this paper, and some necessary constraints should be considered to ensure the safety requirements, such as power balance constraints, constraints of PEVs and upper and state of charge (SoC) limit of battery etc. In addition, due to the uncertainties, the access of PEVs and DGs will alter the balance of the power grid. Therefore, the constraints of themselves and how they affect the traditional power grid should be taken into account.

### 2.1. Description of MESS

The proposed MESSs architecture is illustrated in Fig. 1, which comprises PV, thermal units, battery energy storage, large number of PEVs, and demand load. The solar-powered photovoltaic panels convert solar energy into electricity and deliver it to the power grid, which contribute to the energy generation component of the MESS. The BESS can release excess electricity stored during daytime to supplement peak energy demand use, when there is a shortage of photovoltaic power. In addition, PEVs are equipped with rechargeable batteries that can be charged and store electricity. The batteries of PEVs can be incorporated

into the power grid to provide or draw electricity from the power system as needed. This bidirectional power supply and energy exchange capability allows PEVs to act as mobile energy storage devices, and provide flexible energy support.

The MESS must balance energy supply (from PV, thermal, and PEVs) and demand (from various loads) efficiently. For example, when there is surplus energy from PV, it can be used to charge the PEVs, provide additional thermal energy, or be stored in the battery for later use. Conversely, when there is a high demand for energy, the system can utilize the stored energy in the battery to meet the demand. This dynamic and real-time coordination of the modules is essential for a well-functioning multi-energy system. Therefore, MESSs require coordination, optimization, and management of multiple modules with different characteristics, dynamics, and requirements, while also taking into account various external factors and constraints.

### 2.2. Objective function

In this paper, the modeled objective function $F$ is comprised of the economic cost of the thermal generating units and distributed energy storage batteries, as well as the carbon emission cost of the units and PEVs. However, the study neglects to account for the interrelationships between hourly expenses. The function is shown as follows:

$$\begin{cases} F = \omega Cost + (1-\omega)\, Emission \\ Cost = min\ (f_{UC} + f_{bat}) \\ Emission = min(f_{UC}^{emi} + f_{PEV}^{emi}) \end{cases} \tag{1}$$

In (1), the cost of generating power from the unit can be separated into two components: the costs of using fossil fuels during the process of units, and the costs of start and stop the units. The costs of carbon emission include the emissions of thermal unit $f_{UC}^{emi}$ and PEVs $f_{PEV}^{emi}$.

$$\begin{cases} f_{UC} = \sum_{t=1}^{T} \sum_{j=1}^{n} (F_j(P_{j,t}) z_{j,t} + ST_{j,t}(1 - z_{j,t-1}) z_{j,t}) \\ f_{bat} = \sum_{t=1}^{T} \sum_{k=1}^{nb} C_{k,t} \times pr \\ f_{UC}^{emi} = \sum_{t=1}^{T} \sum_{j=1}^{n} F_j^{emi}(P_{j,t}) z_{j,t} \times pr_e \\ f_{PEV}^{emi} = \sum_{t=1}^{T} \sum_{p=1}^{np} E_p^{PEV} \times pr_e \end{cases} \tag{2}$$

where $P_{j,t}$ is the amount of electricity generated by the $j$th unit in hour $t$. The costs of the fossil fuels depleted during the operation of the units is indicated by $F_j(P_{j,t})$. $F_j^{emi}(P_{j,t})$ represents the function that the cost associated with carbon emissions generated by the units. $C_{k,t}$ is the capacity of energy storage $k$th battery at each hour. $E_p^{PEV}$ represents the total capacity of PEVs. $pr$ and $pr_e$ represent the price of battery installation cost and the average trade price of emissions, respectively, suggested by [58]. $\omega$ is the coefficient of balancing economy and carbon emissions, which is set to 0.3 in this paper, and the detailed analysis can been seen in Section 5.

The fuel cost function and the emission cost function are demonstrated in Eq. (3) and (4):

$$F_{j,t}(P_{j,t}) = a_j + b_j P_{j,t} + c_j P_{j,t}^2 \tag{3}$$

$$F_{j,t}^{emi}(P_{j,t}) = \alpha_j + \beta_j P_{j,t} + \gamma_j P_{j,t}^2 \tag{4}$$

where $a_j$, $b_j$ and $c_j$ represent the fuel constants of the $j$th unit. $\alpha_j$, $\beta_j$ and $\gamma_j$ represent $CO_2$ emission constants of the $j$th unit.

Considering the characteristics of the unit itself, most generators may need to adjust the operating state, such as not turning on immediately after shutdown. The start–stop unit consumes more fuel under the starting condition, so the start-up cost should be considered in the economic cost, which can be expressed as $ST_{j,t}(1 - z_{j,t-1})z_{j,t}$, and the formula is modeled as below.

$$ST_{j,t} = \begin{cases} ST_j^{hot},\ if\ MDT_j \le CDT_{j,t} \le MDT_j + T_{cold,j} \\ ST_j^{cold},\ if\ CDT_{j,t} > MDT_j + T_{cold,j} \end{cases} \tag{5}$$

where $z_{j,t}$ represents whether the $j$th unit is currently in the on or off state at time $t$, where the on state is symbolized by 1 and the off is 0. If the unit was off in the previous time interval but is now on, the startup cost is incurred and is set to 0 in all other cases. The startup cost can be classified as either hot start cost or cold start cost, depending on the duration of time the unit has been inactive before being restarted. $CDT_{j,t}$ and $MDT_j$ represent the continuous shutdown time and the minimum down time of the $j$th unit, respectively. The limitation of cold start time is represented by $T_{cold,j}$. $ST_j^{hot}$ and $ST_j^{cold}$ represent the hot start mode and the cold start mode, respectively. If the downtime of the unit exceeds $MDT_j$ and is less than $MDT_j + T_{cold,j}$, then the unit is considered to be in hot start mode, and vice versa.

### 2.3. Constraints of the proposed problem

Determining the number of online units required during various time periods involves taking into account a variety of parameters in order to optimize performance. These factors include the limitations of individual units and the interactions between units at different times. Meeting these constraints is essential to achieve the optimal economic cost objective. Additionally, the influence of DGs and PEVs is also considered in constraints.

#### 2.3.1. Power balance constraints

The demand for electricity in industrial power generation is constantly changing. In addition, the integration of DGs and PEVs into the power grid may have an impact on the energy structure of the grid, so the power balance constraints need to be considered, which can be indicated by the following equation:

$$\sum_{j=1}^{n} P_{j,t} z_{j,t} + \underbrace{P_{PV,t} + P_{Bat,t}}_{DGs} = P_{D,t} + P_{PEV,t} \tag{6}$$

In (6), the power generated by the whole units at hour t is defined as $\sum_{j=1}^{n} P_{j,t} z_{j,t}$, $P_{D,t}$ is the traditional demand load at time t, the distributed energy storage system consists of $P_{PV,t}$ and $P_{Bat,t}$, which represent the Photovoltaic connected to the grid and the output power of batteries for supply side at hour t, respectively. $P_{PEV,t}$ represents the load demand of PEVs during hour $t$, which can function in two modes: grid-to-vehicle (G2V) and vehicle-to-grid (V2G) [59]. The PEVs draw power from the grid to charge or involve the capability of PEVs to supply power back to the power grid when needed. In simpler terms, the demand power of PEVs is represented by a positive number, and the supply power of PEVs is represented by a negative number for grid services.

#### 2.3.2. Constraints of generating capacity

Considering the physical constraints of generation units, it is necessary to account for the maximum and minimum bounds of their generating capacity. Meanwhile, since the DGs are integrated with UC, the maximum and minimum bounds of photovoltaic and batteries are also taken into account, which apply the following constraints:

$$z_{j,t} P_{j,min} \le P_{j,t} \le z_{j,t} P_{j,max} \tag{7}$$

$$0 \le P_{PV,t} \le P_{PV,max} \tag{8}$$

$$P_{Bat,min} \le P_{Bat,t} \le P_{Bat,max} \tag{9}$$

In (7), $P_{j,min}$ and $P_{j,max}$ represent the maximum and minimum bounds of the power generated by the $j$th unit, respectively. The generation capacity of photovoltaic is mainly affected by the external environment such as solar radiation, and the scale of installed capacity, this study the installed capacity of the photovoltaic is set in the range of [0, $P_{PV,max}$], which is shown in (8). $P_{Bat,min}$ and $P_{Bat,max}$ denote the maximum capacity [MW] and minimum capacity [MW] of the battery, respectively.

#### 2.3.3. Spinning reserve constraints

In practical situations, reserving enough potential power is necessary to ensure that power demands are met and balance grid load fluctuations and load prediction errors. This is mathematically represented as below.

$$\sum_{j=1}^{n} P_{j,max} z_{j,t} + P_{PV,t} + P_{Bat,t} \geq P_{D,t} + P_{PEV,t} + SR_t \tag{10}$$

$$SR_t = m \times P_{D,t}. \tag{11}$$

where $SR_t$ represents the spinning reserve at each hour, and the corresponding formula is shown in (11). The total capacity generated by the units and DGs should be greater than or equal to the overall demand loads, which are the electrical demands of all customers connected to the system, plus the spinning reserves to maintain a reliable power supply. This paper adopts the recommendation from [60] to set the spinning reserve at 0.1 times the conventional load.

#### 2.3.4. Minimum up or down time of units

The unit's shutdown and startup require a specific amount of time and cost. If the starting and shutdown time intervals are too short, the unit will restart and shut down frequently increasing energy consumption and cost. The working period of the unit can be sensibly arranged to decrease energy waste and cost by taking the constraints into account, which is calculated by

$$z_{j,t} = \begin{cases} 1, & if\ 1 \leq CUT_{j,t-1} < MUT_j \\ 0, & if\ 1 \leq CDT_{j,t-1} < MDT_j \\ 0\ or\ 1, & otherwise \end{cases} \tag{12}$$

In (12), switch status of the unit is represented by 0 and 1, respectively, where $MUT_j$ and $MDT_j$ refer to the minimum duration for which the unit is on and off, respectively. $CUT_{j,t-1}$ represents the continuously starting up time and $CDT_{j,t-1}$ represents the continuously shutting down time of units. If the unit remains in the startup state for a duration shorter than the required minimum up time, it should stay in that condition, and vice versa.

#### 2.3.5. Constraints of PEVs

Given that the demand for PEVs charging is unpredictable, it is crucial to consider their limitations and restrictions in order to maintain the grid's steady functioning. These constraints include the maximum charging and discharging capacity constraints, as well as the power requirement restrictions of the PEVs, which can be expressed using Eqs. (13) and (14), respectively.

$$P_{PEVD,t,max} \leq P_{PEV,t} \leq P_{PEVC,t,max} \tag{13}$$

where $P_{PEVD,t,max}$ and $P_{PEVC,t,max}$ denote the maximum discharge capacity and the maximum charge capacity of the whole PEVs during each hour, respectively.

$$\sum_{t=1}^{T} P_{PEV,t} = P_{PEV,total} \tag{14}$$

The Eq. (14) indicates the total electricity requirement necessary to sustain the regular execution of PEVs over a single day. Meanwhile, $P_{PEV,total}$ denotes the overall charging demand loads of the whole PEVs within that day.

#### 2.3.6. State of charge limit of battery

Due to the physical material of the battery in energy storage system, its SoC needs to be considered, the reason is that the over-discharging and overcharging can both reduce their longevity. Therefore, it is necessary to set a reasonable range for the SoC of the battery, which can be described as:

$$SoC_{min} \leq SoC_{k,t} \leq SoC_{max} \tag{15}$$

where $SoC_{min}$ represents the minimum state of charge limit of all batteries in energy storage system, which is set to 10%, and $SoC_{max}$ represents the maximum state of charge limit, which is set to 100%.

## 3. Methodology

The proposed system model of units integrated with DGs and PEVs has the characteristics of high dimensionality, multi-modality, strong coupling, and great nonlinearity, which makes traditional optimization algorithms difficult to optimize. This paper proposed the binary level-based learning swarm optimization framework to tackle this problem.

### 3.1. Original level-based learning swarm optimization

The computational complexity involved with addressing the MESSs scheduling problem increases as its dimension develops. Simultaneously, the search space, which encompasses all possible solutions to the problem, expands exponentially, becoming increasingly challenging to explore thoroughly. For the strong-coupling high-dimensional problems, the optimization algorithms of SLPSO [61] and CSO [62] utilize superior individuals in the current population to update other individuals, which results in improved diversity and makes them effective in addressing problems with a high number of dimensions. However, these two optimizers only select one superior individual to guide the update of individuals and all individuals share the average position of the population, which hinders the potential for enhancing diversity during each update process.

The level-based learning mechanism is employed by level-based learning swarm optimization (LLSO), which involves dividing the particles into various levels. In addition, it leverages the knowledge of the two best-performing individuals in the population to instruct the learning processes of other individuals, thereby improving their ability to locate the global optimum. Moreover, the scheduling optimization for MESSs involves a nonlinear mixed-integer problem. The binary decision variables are associated with the activation and deactivation of generating units. In contrast, the integration of PEVs load management and DRGs power generation entails decimal values. Hence, an improved LLSO is developed to optimize the on–off status of the units in this paper to align with practical requirements.

### 3.2. Improved LLSO

Firstly, the individuals in the population are arranged according to the ascending order of fitness values, the same as SLPSO. Then, they are equally separated into different levels (L1, L2, L3 and L4), each individual selects two random individuals from two different higher levels to update its position.

After the fitness values have been determined and sorted, let us assume that the population $N$ is divided into M levels, each level being denoted by $L_m = [L_1, L_2, \ldots, L_M]$. The higher the level, the better the individuals are, and the smaller the level index it has. Such as the individuals from $L_3$ are better than the individuals from $L_4$. The size of the level is defined as S, S = N/M. It is important to highlight that for the purpose of preventing the most promising individuals from being updated incorrectly, the individuals in $L_1$ are exempt from updates and are directly carried forward to the next generation. The learning strategy to update population position with LLSO is determined by the following:

$$\mathbf{X}^d(t+1) = \begin{bmatrix} x^d_{1,1} + v^d_{1,1}(t+1) & x^d_{1,2} + v^d_{1,2}(t+1) & \ldots & x^d_{1,S} + v^d_{1,S}(t+1) \\ x^d_{2,1} + v^d_{2,1}(t+1) & x^d_{2,2} + v^d_{2,2}(t+1) & \ldots & x^d_{2,S} + v^d_{2,S}(t+1) \\ \vdots & & \ddots & \\ x^d_{M,1} + v^d_{M,1}(t+1) & x^d_{M,2} + v^d_{M,2}(t+1) & \ldots & x^d_{M,S} + v^d_{M,S}(t+1) \end{bmatrix} \tag{16}$$

In (16), $\mathbf{X}^d(t+1)$ represents the population of the $d$th dimension. Each individual updates the position according to (17) and (18).

$$x^d_{i,j}(t+1) = x^d_{i,j} + v^d_{i,j}(t+1) \tag{17}$$

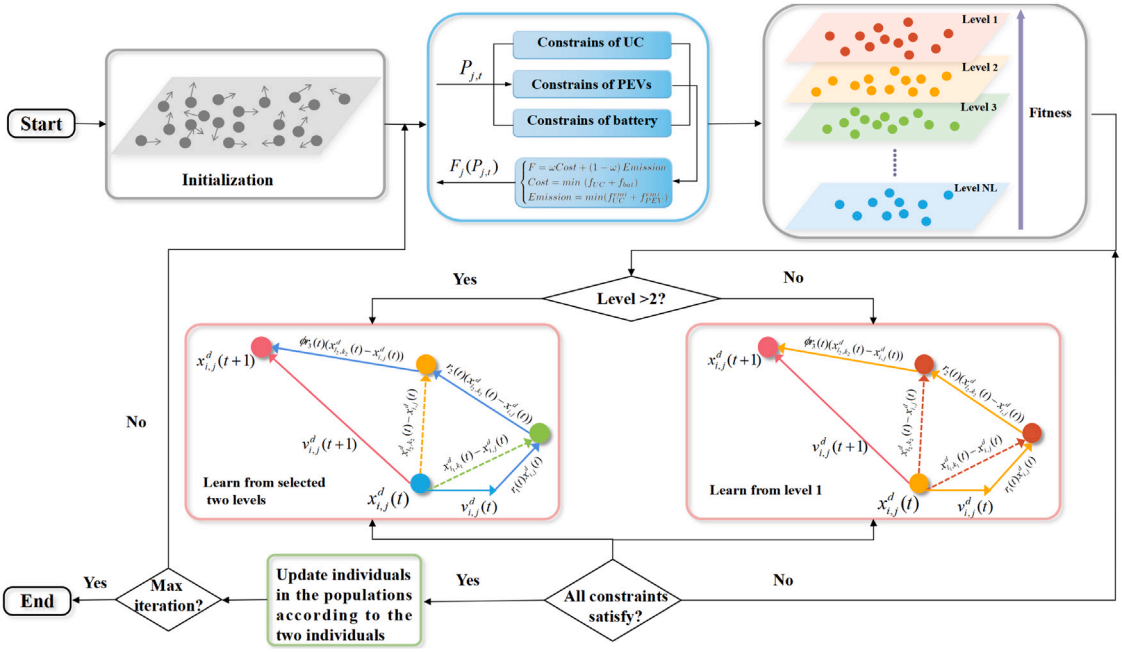


**Fig. 2.** The algorithm flowchart of BLLSO.

where $x_{i,j}^d(t)$ denotes the position of the $j$th individual of the $d$th dimension from the $i$th level $L_i$, and $v_{i,j}^d(t)$ is its velocity at generation t.

$$v_{i,j}^d(t+1) = r_1(t)v_{i,j}^d(t) + r_2(t)\Delta x_{l_1,j}^d(t) + \phi r_3(t)\Delta x_{l_2,j}^d(t) \tag{18}$$

with

$$\begin{cases} \Delta x_{l_1,j}^d(t) = x_{l_1,k_1}^d(t) - x_{i,j}^d(t) \\ \Delta x_{l_2,j}^d(t) = x_{l_2,k_2}^d(t) - x_{i,j}^d(t) \\ \phi = 0.01 \times \frac{n}{m} \end{cases} \tag{19}$$

In (18), $\Delta x_{l_1,j}^d(t)$ and $\Delta x_{l_2,j}^d(t)$ are what the individual learns from two different predominant individuals at each generation. $x_{l_1,j}^d(t)$ and $x_{l_2,j}^d(t)$ represent two selected individuals from two different selected levels, $L_{l1}$ and $L_{l2}$, $l_1$ and $l_2$ are level indexes from two different higher levels within [1, i-1], respectively. The indexes $k_1$ and $k_1$ are randomly chosen from the range [1, LS] to represent two different individuals. $r_1(t)$, $r_2(t)$ and $r_3(t)$ represent all parameters randomly selected from [0,1]. $\phi$ is the influence factor to control the $\Delta x_{l_2,j}^d(t)$, which is determined by characteristics such as population scale and dimension, and influences the degree of update for the current individual based on its learning from an inferior one. It is worth noting that the index of $L_2$ is greater than the index of $L_1$, and both are higher than the index of $L_i$.

Since the status of the unit to be optimized in the update process is a binary variable, and the updated particle velocity value is a decimal variable, in order to make each attribute of the particle have the same encoding method in the update strategy, the V-shaped function is employed in this paper to discretely process the particles at each updated position, the converted LLSO update mechanism is as follows:

$$x_{i,j}^d(t+1) = x_{i,j}^d + BC(v_{i,j}^d(t+1)) \tag{20}$$

$$BC(v_{i,j}) = 2 * |\frac{1}{1+e^{-v_{i,j}}} - 0.5| \tag{21}$$

from (21), it can be seen that the velocity $v$ of the particle has a great decisive effect on the result of discretization. If the velocity value is either too large or too small, it is easy to cause the position of the individual to be concentrated on 0 or 1, so the range of the particle speed is set to [−4,4] in this paper. The corresponding position update of the individual is as follows:

$$x_{i,j} = \begin{cases} 1, & \text{if } rand < BC(v_{i,j}) \\ 0, & \text{otherwise} \end{cases} \tag{22}$$

where $x_{i,j}$ represents the update position of individual after converted, *rand* can generate random numbers ranging within [0,1]. If $BC(v_{i,j})$ is bigger than the random integer *rand*, then the particle's position attribute value is set to 1, indicating that the unit is in the power-on state in the UC problem, otherwise, the position attribute value of the particle is 0, that is, it is in the power-off state.

The level-based learning mechanism might encourage higher-level learners to engage in more exploitation while lower-level learners engage in more exploration. On the one hand, it can give rise to a potential balance between exploitation and exploration for each individual. On the other hand, the unpredictability properties of level selection and dominant individual selection contributes to the enhancement of diversity, which is a crucial factor in large-scale optimization problems. In Fig. 2, the algorithm flowchart of BLLSO is displayed, we will discuss the performance of the algorithm and set some specific parameters in Section 4.

### 3.3. The specific stages of the proposed algorithm

As the quantity of PEVs continues to increase, large-scale PEVs charging demand could place pressure on the grid, so effective management strategies are required to ensure the energy balance and enhance the reliability and effectiveness of the electrical grid. Simultaneously, photovoltaics and batteries are integrated into the grid as distributed energy storage, which will cause the instability in the power supply, due to the uncertainty of different energy. Based on the above questions, a binary level-based learning swarm optimization method is proposed and the proposed MESSs scheduling framework is summarized in Fig. 3. And the specific stages of the proposed MESSs optimization algorithm for UC problems integrated with DGs and PEVs is as follows:

(1) *Data Initialization:* Firstly, input and initialize the relevant data of the units and the real charging information of the PEVs around the

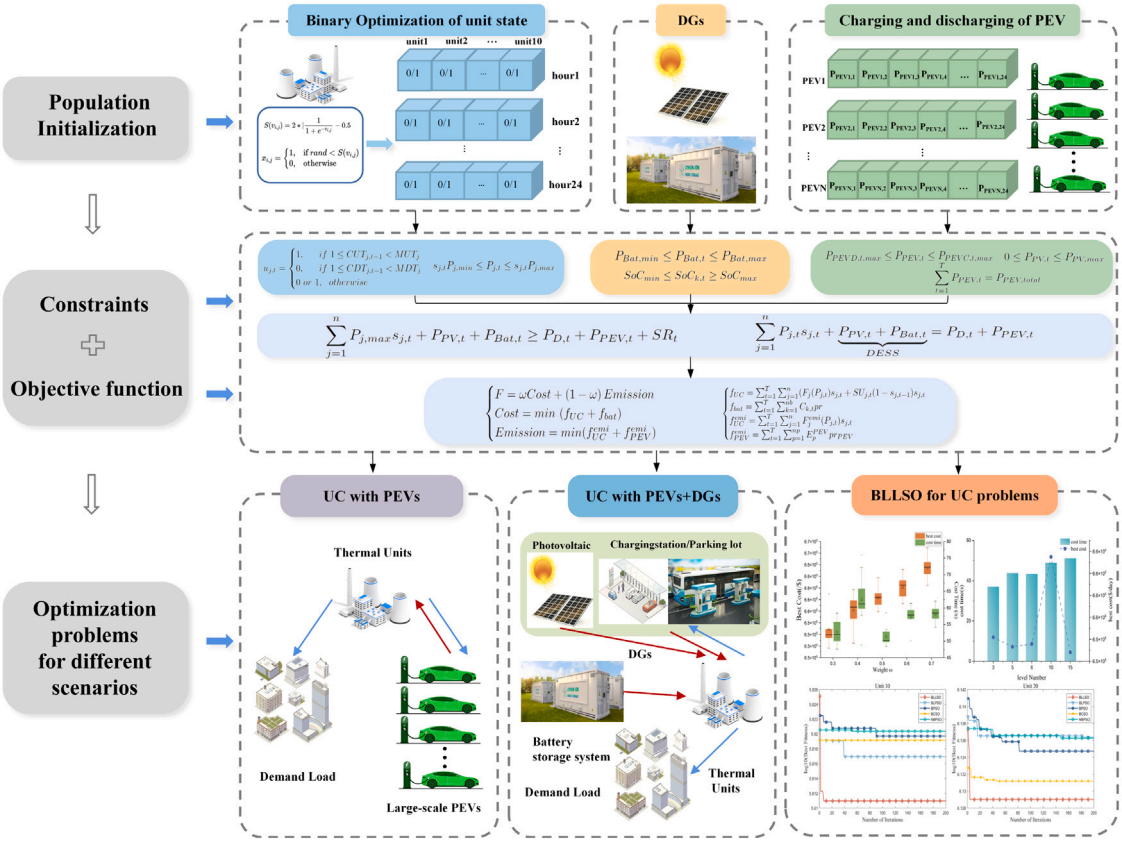


**Fig. 3.** The proposed MESSs scheduling framework.

clock, some necessary parameters should also be initialized, such as maximum/minimum power generation output, hot or cold start cost, fuel coefficients, and the initial state of the unit. The range of particle velocity and algorithm parameters that exist during the optimization algorithm are also objects that need to be initialized.

(2) *Constraint Handling:* So as to ensure the effectiveness and accuracy of the optimization process, constraint handling is an essential process. The unit data after initialization should satisfy the minimum up/down-time limit, otherwise, the on–off state of the unit will be modified to the limited boundary value. The data of PEVs should satisfy the constraint conditions (13) and (14). The battery should meet the limit of SoC to avoid the over discharging and overcharging.

(3) *Fitness Calculation:* According to formula (1), calculate the fitness value of each particle, and the lambda iteration method [19] is considered to obtain the output of each unit. Note that different scenarios may have different objective functions, details shown in Section 4.

(4) *Individual stratification:* After calculating the fitness values of all particles, sort them in ascending order, and then stratify all particles according to their fitness values. What needs to be reminded is that the individuals at the level $L_1$ enter the following iteration without updating or learning, so as to prevent the most potential individuals from being incorrectly updated. The individuals at the level $L_2$ update the positions in accordance with two predominant individuals, which are both from the level $L_1$.

(5) *Population update:* The optimization algorithm of BLLSO is conducted to optimize the positions of all individuals according to the fitness values, and the particles whose positions have been updated still need to judge whether the constraints are satisfied.

(6) *Judging the termination condition:* If the value of current iteration is smaller than the value of termination iteration, continue to step (3) – (5). Otherwise, return the optimized result and stop the procedure.

## 4. Numerical studies and results analysis

Different Scenarios are considered to confirm the efficiency and feasibility of the proposed optimal framework, in this section. The first scenario aims to explore the validity of the charge and discharge management of PEVs on the grid, with the goal of reducing peak and valley demand. The main focus of the second scenario is to analyze the performance of the proposed MESSs, as well as to address the role and potential benefits of each module in the grid. The last scenario demonstrates the superiority of the LLSO algorithm in resolving the UC problems under different circumstances involving various numbers of units. This is accomplished by a comparative analysis of its performance against four other algorithms.

### 4.1. Experimental setup

The data of PEVs was obtained on the charging demand of 50,000 electric vehicles in Shenzhen, Guangdong Province, China, on a typical 24-hour day. All experimental results are conducted on a PC with 12th Gen Intel(R) Core(TM) i7-12700 2.10 GHz CPUs, 32 GB RAM, and a platform with Matlab R2022b. The parameter configurations of the generation units employed in this paper were based on [63], and the details are provided in Table 1. Moreover, it is worth noting that as the number of units increases, so will the dimension of the system to be optimized. When the quantity of units is 10, the variable dimension is 240; when the unit size is increased to 100, the variable dimension is 2400.

### 4.2. The influence of management of PEVs charge and discharge on UC problems

This section investigates the impact of electric vehicles charge and discharge management integrated into the electrical grid. On the one

**Table 1**
UC model parameter settings.

| | Unit1 | Unit2 | Unit3 | Unit4 | Unit5 | Unit6 | Unit7 | Unit8 | Unit9 | Unit10 |
|---|---|---|---|---|---|---|---|---|---|---|
| Pmax(MW) | 455 | 455 | 130 | 130 | 162 | 80 | 85 | 55 | 55 | 55 |
| Pmin(MW) | 150 | 150 | 20 | 20 | 25 | 20 | 25 | 10 | 10 | 10 |
| a($ /h) | 1000 | 970 | 700 | 680 | 450 | 370 | 480 | 660 | 665 | 670 |
| b($ /MWh) | 16.19 | 17.26 | 16.6 | 16.5 | 19.7 | 22.26 | 27.74 | 25.92 | 27.27 | 27.79 |
| c($ /MW$^2$h) | 0.00048 | 0.00031 | 0.002 | 0.00211 | 0.00398 | 0.00712 | 0.00079 | 0.00413 | 0.00222 | 0.00173 |
| $\alpha$(ton/h) | 103.3908 | 103.3908 | 300.3910 | 300.3910 | 320.0006 | 320.0006 | 330.0056 | 330.0056 | 350.0056 | 360.0012 |
| $\beta$ (ton/MW h) | −2.4444 | −2.4444 | −4.0695 | −4.0695 | −3.8132 | −3.8132 | −3.9023 | −3.9023 | −3.9524 | −3.9864 |
| $\gamma$(ton/MW$^2$h) | 0.0312 | 0.0312 | 0.0509 | 0.0509 | 0.0344 | 0.0344 | 0.0465 | 0.0465 | 0.0465 | 0.047 |
| MUT(h) | 8 | 8 | 5 | 5 | 6 | 3 | 3 | 1 | 1 | 1 |
| MDT(h) | 8 | 8 | 5 | 5 | 6 | 3 | 3 | 1 | 1 | 1 |
| $SU_H$($) | 4500 | 5000 | 550 | 560 | 900 | 170 | 260 | 30 | 30 | 30 |
| $SU_C$($) | 9000 | 10 000 | 1100 | 1120 | 1800 | 340 | 520 | 60 | 60 | 60 |
| $T_{cold}(h)$ | 5 | 5 | 4 | 4 | 4 | 2 | 2 | 0 | 0 | 0 |
| Initial Status(h) | 1 | 1 | 0 | 0 | 0 | 0 | 0 | 0 | 0 | 0 |

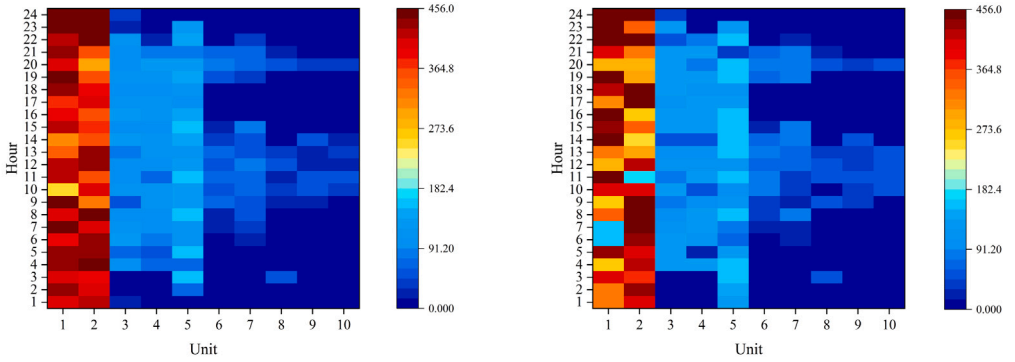


(a) The output heat map of 10 units (b) The output heat map of 10 units integrated with PEVs

**Fig. 4.** Heat map comparison of unit output under different scenarios.

hand, PEVs provide a variable load that may be programmed to charge during off-peak times when power consumption is lower, which can assist control the load on the grid and aid the grid balance to meet peak demand. On the other hand, batteries play a crucial role in distributed energy storage systems as they enable the storage of excess energy when it is available and release it when the demand is high, which contributes to better power grid stability.

In this paper, it is assumed that the integration model of 10 units with a total of 150,000 PEVs, the battery capacity of PEVs is set to 30 KWh [64], the maximum power of energy storage batteries is 5 MW [65], and the total load of PEVs is about 1.114 GWh. Furthermore, the maximum charge and discharge power of PEVs is 153 MW and −153 MW, respectively, where the available SOC of PEVs is 50%, the proportion of available PEVs quantity per hour is 20

The optimal results of charge and discharge management of PEVs integrated into the electric system are displayed in Table 2 and Fig. 7 case 1. According to Table 2, the peak period of power demand is from 9:00 am to 14:00, and from 20:00 to 21:00 pm, and the peak power generation periods of the units are also focused on these periods. Moreover, when the load is in the peak period, the PEVs discharge to satisfy the electricity demand, and when the load is in the valley period, the PEVs can charge, thus illustrating the effectiveness of the proposed optimization algorithm for the charge and discharge management of the PEVs, and PEVs can realize valley-shaving and peak-filling to steady the power demand. Moreover, Fig. 4 illustrates the comparison of unit output with and without PEVs. From Fig. 4(a), it is clear that in the case of no PEVs integration, compared with other units, Unit 1 and 2 are burdened with heavy output and unbalanced load distribution over a 24-hour period compared to other units. In contrast, Fig. 4(b) demonstrates that the PEVs integration into the grid significantly reduce the output burden for the units and make the overall power system more stable.

### 4.3. Uncertainty analysis of proposed MESSs

Due to the generation of PV is intermittent and variable, the charging and discharging behavior of PEV is random, which can be challenging for the balance of the grid. In order to effectively evaluate the uncertainty of renewable energy and electric vehicles, this paper utilizes the Latin hypercube sampling (LHS) method [66] to generate multi-dimensional parameter space random samples.

In this section, the MESSs with 10 units is considered, and 10 scenarios are randomly generated to simulate random photovoltaic power generation and PEVs charging and discharging to analyze the impact of uncertainty on the MESSs. The analysis of Fig. 5(a) indicates that there is a discernible escalation in power demand across all scenarios at specific intervals, notably prior to 7 a.m. and subsequent to 8 p.m. These surges are indicative of conventional electricity consumption patterns that correspond with the morning and evening rush hours, coinciding with the populace commencing and concluding their work-related activities. Different from highly random PEVs, the PV power generation profile presented in Fig. 5(b) demonstrates a pronounced regularity that is synchronous with the diurnal cycle of sunrise and sunset, so meteorological conditions are a crucial determinant of the actual energy yield from photovoltaic. Consequently, it can be substantiated that this method is efficacious in examining the stochastic characteristics of PEV power demand and the intermittency inherent in photovoltaic power generation. Concurrently, the analysis confers advantages to the power grid management by facilitating accurate forecasts of power demand and enabling the implementation of requisite adjustments to accommodate the extensive adoption of PEVs and photovoltaics.

Tables 3 and 4 offer a comparative analysis of the economic costs associated with the operation of MESS under two distinct operational

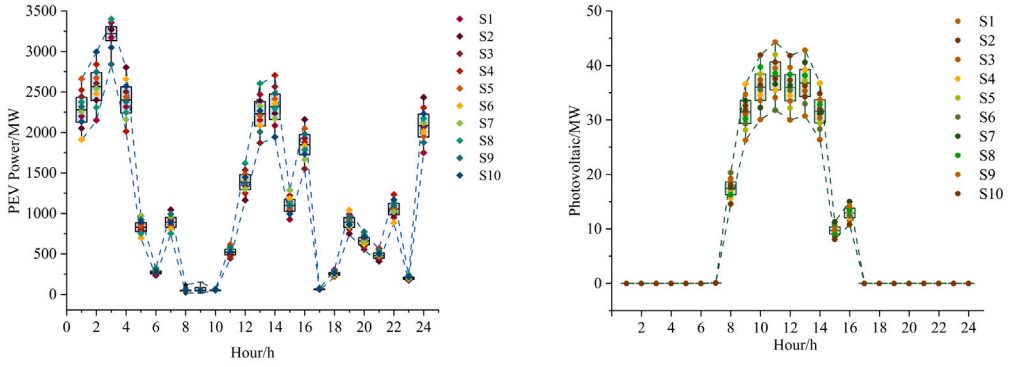


(a) The random scenario generation of PEVs. (b) The random scenario generation of photovoltaic power.

**Fig. 5.** Scenario generation comparison of MESSs under 10 units.

**Table 2**
The optimal results of charge and discharge management of PEVs in UC problems.

| Hour | Unit1 (MW) | Unit2 (MW) | Unit3 (MW) | Unit4 (MW) | Unit5 (MW) | Unit6 (MW) | Unit7 (MW) | Unit8 (MW) | Unit9 (MW) | Unit10 (MW) | Demand (MW) | PEV Load (MW) |
|---|---|---|---|---|---|---|---|---|---|---|---|---|
| 1 | 382.78 | 450.22 | 0.00 | 20.00 | 0.00 | 0.00 | 0.00 | 0.00 | 0.00 | 0.00 | 700.00 | 153.00 |
| 2 | 398.20 | 455.00 | 0.00 | 49.80 | 0.00 | 0.00 | 0.00 | 0.00 | 0.00 | 0.00 | 750.00 | 153.00 |
| 3 | 455.00 | 454.43 | 73.57 | 20.00 | 0.00 | 0.00 | 0.00 | 0.00 | 0.00 | 0.00 | 850.00 | 153.00 |
| 4 | 418.16 | 453.57 | 85.00 | 45.19 | 101.07 | 0.00 | 0.00 | 0.00 | 0.00 | 0.00 | 950.00 | 153.00 |
| 5 | 412.12 | 444.87 | 20.00 | 99.36 | 162.00 | 0.00 | 0.00 | 0.00 | 0.00 | 0.00 | 1000.00 | 138.35 |
| 6 | 439.85 | 384.14 | 117.58 | 129.40 | 88.47 | 0.00 | 0.00 | 10.00 | 0.00 | 0.00 | 1100.00 | 69.44 |
| 7 | 392.50 | 408.37 | 130.00 | 127.71 | 162.00 | 0.00 | 40.71 | 10.00 | 0.00 | 0.00 | 1150.00 | 121.29 |
| 8 | 381.74 | 409.84 | 107.39 | 130.00 | 126.88 | 48.02 | 61.57 | 0.00 | 0.00 | 0.00 | 1200.00 | 65.44 |
| 9 | 372.42 | 401.10 | 105.27 | 92.73 | 108.92 | 75.95 | 37.22 | 36.08 | 0.00 | 10.93 | 1300.00 | −59.38 |
| 10 | 404.25 | 387.05 | 79.35 | 130.00 | 92.46 | 58.09 | 77.22 | 30.41 | 52.57 | 18.29 | 1400.00 | −70.30 |
| 11 | 415.26 | 378.98 | 130.00 | 92.02 | 150.86 | 39.63 | 68.57 | 25.71 | 37.60 | 35.34 | 1450.00 | −76.03 |
| 12 | 336.21 | 434.00 | 105.49 | 130.00 | 122.98 | 66.40 | 85.00 | 10.00 | 46.92 | 10.00 | 1500.00 | −153.00 |
| 13 | 450.48 | 379.66 | 72.46 | 89.31 | 103.81 | 54.22 | 57.92 | 16.69 | 35.38 | 45.89 | 1400.00 | −94.19 |
| 14 | 406.35 | 389.92 | 110.20 | 70.01 | 100.58 | 56.03 | 63.77 | 33.78 | 19.57 | 0.00 | 1300.00 | −49.79 |
| 15 | 423.86 | 435.71 | 78.88 | 111.27 | 138.06 | 20.00 | 69.74 | 0.00 | 0.00 | 0.00 | 1200.00 | 77.53 |
| 16 | 435.27 | 385.01 | 130.00 | 84.02 | 82.29 | 0.00 | 25.00 | 0.00 | 0.00 | 0.00 | 1050.00 | 91.61 |
| 17 | 396.05 | 378.94 | 43.34 | 105.00 | 123.93 | 0.00 | 25.00 | 0.00 | 0.00 | 0.00 | 1000.00 | 72.26 |
| 18 | 455.00 | 328.27 | 96.41 | 105.60 | 162.00 | 0.00 | 25.00 | 0.00 | 0.00 | 0.00 | 1100.00 | 72.28 |
| 19 | 404.33 | 438.53 | 128.99 | 98.68 | 109.06 | 60.42 | 25.00 | 0.00 | 0.00 | 0.00 | 1200.00 | 65.02 |
| 20 | 384.33 | 399.42 | 120.74 | 84.37 | 93.83 | 45.24 | 67.76 | 20.30 | 41.06 | 46.70 | 1400.00 | −96.24 |
| 21 | 421.54 | 379.37 | 102.90 | 75.65 | 67.68 | 80.00 | 85.00 | 10.00 | 20.56 | 0.00 | 1300.00 | −57.30 |
| 22 | 398.00 | 455.00 | 45.00 | 115.92 | 110.32 | 0.00 | 0.00 | 55.00 | 0.00 | 0.00 | 1100.00 | 79.23 |
| 23 | 455.00 | 455.00 | 0.00 | 80.00 | 63.00 | 0.00 | 0.00 | 0.00 | 0.00 | 0.00 | 900.00 | 153.00 |
| 24 | 455.00 | 437.75 | 0.00 | 0.00 | 60.25 | 0.00 | 0.00 | 0.00 | 0.00 | 0.00 | 800.00 | 153.00 |

**Table 3**
Economic cost comparison of MESS with PEVs and BESS.

| Scenario | UC+PEV | | | | UC+PEV+BESS | | | |
|---|---|---|---|---|---|---|---|---|
| | Best | Worst | Mean | Std | Best | Worst | Mean | Std |
| S1 | 647 388.64 | 653 603.65 | 650 496.15 | 4394.68 | 665 572.81 | 666 484.32 | 666 028.56 | 644.53 |
| S2 | 648 506.12 | 650 687.94 | 649 597.03 | 1542.78 | 664 187.57 | 668 720.69 | 666 454.13 | 3205.40 |
| S3 | 647 739.10 | 652 217.38 | 649 978.24 | 3166.63 | 662 696.90 | 665 028.74 | 663 862.82 | 1648.85 |
| S4 | 649 446.66 | 650 336.69 | 649 891.68 | **629.35** | 662 305.06 | **663 093.87** | 662 699.46 | 557.77 |
| S5 | **642 012.33** | 651 985.17 | 646 998.75 | 7051.87 | 662 337.04 | 666 492.47 | 664 414.76 | 2938.33 |
| S6 | 648 150.12 | 649 885.46 | 649 017.79 | 1227.07 | **656 518.51** | 666 721.72 | **661 620.11** | 7214.75 |
| S7 | 644 885.02 | 647 561.15 | 646 223.09 | 1892.31 | 665 088.08 | 665 536.15 | 665 312.11 | **316.83** |
| S8 | 642 490.86 | **647 106.92** | **644 798.89** | 3264.05 | 662 651.44 | 667 551.91 | 665 101.67 | 3465.16 |
| S9 | 649 059.24 | 651 199.52 | 650 129.38 | 1513.41 | 662 032.01 | 666 764.82 | 664 398.42 | 3346.59 |
| S10 | 645 736.49 | 649 733.98 | 647 735.24 | 2826.65 | 664 246.01 | 666 037.63 | 665 141.82 | 1266.86 |

scenarios: PEV scenario and the Photovoltaic scenario. The scenarios enumerated reflect a variety of MESS operational conditions that were generated using the LHS method. Empirical observations reveal that the economic costs incurred in the PEV scenario are markedly lower than those in the PV scenario. This disparity is likely attributable to the inherent intermittency of photovoltaic energy generation, which compromises stability relative to the PEV scenario. Notwithstanding the scenario, it is noteworthy that the incorporation of BESS engenders an augmentation in economic costs. This increment can be primarily ascribed to the capital expenditure required for BESS installation. However, the integration of BESS appears to mitigate the variability of economic costs, as evidenced by the reduction in the standard deviation. Specifically, the optimal standard deviation in Table 3 with BESS integration is reduced by 312.52 $/day compared to the system without BESS. Similarly, in Table 4, the reduction is 514.02 $/day. This diminution in standard deviation underlines the potential of BESS

**Table 4**
Economic cost comparison of MESS with photovoltaic and BESS.

| Scenario | UC+PV | | | | UC+PV+BESS | | | |
|---|---|---|---|---|---|---|---|---|
| | Best | Worst | Mean | Std | Best | Worst | Mean | Std |
| S1 | **564 963.30** | 578 588.54 | **571 775.92** | 9634.49 | 586 661.62 | 594 626.94 | 590 644.28 | 5632.32 |
| S2 | 575 191.18 | 584 599.99 | 579 895.59 | 6653.03 | **586 020.88** | 594 113.40 | **590 067.14** | 5722.28 |
| S3 | 574 034.24 | **578 582.63** | 576 308.44 | 3216.19 | 593 015.23 | 593 684.00 | 593 349.61 | 472.89 |
| S4 | 574 399.62 | 583 692.32 | 579 045.97 | 6570.93 | 593 716.91 | 595 346.75 | 594 531.83 | 1152.46 |
| S5 | 577 358.98 | 580 947.11 | 579 153.04 | 2537.18 | 592 458.64 | **593 053.58** | 592 756.11 | **420.68** |
| S6 | 577 478.96 | 591 066.97 | 584 272.97 | 9608.17 | 593 293.32 | 595 431.31 | 594 362.31 | 1511.78 |
| S7 | 582 071.00 | 584 405.47 | 583 238.23 | 1650.72 | 591 695.53 | 593 784.01 | 592 739.77 | 1476.77 |
| S8 | 579 810.14 | 586 513.41 | 583 161.78 | 4739.92 | 592 521.90 | 597 920.51 | 595 221.20 | 3817.39 |
| S9 | 579 836.54 | 586 517.78 | 583 177.16 | 4724.35 | 595 222.40 | 600 189.39 | 597 705.89 | 3512.19 |
| S10 | 583 109.88 | 584 431.75 | 583 770.81 | **934.70** | 592 787.62 | 597 743.97 | 595 265.79 | 3504.66 |

**Table 5**
Scenario settings.

| Case | Scenario description |
|---|---|
| Case 1 | UC model integrated with PEVs |
| Case 2 | UC model integrated with PEVs and PV |
| Case 3 | UC model integrated with PEVs, PV and battery storage system |

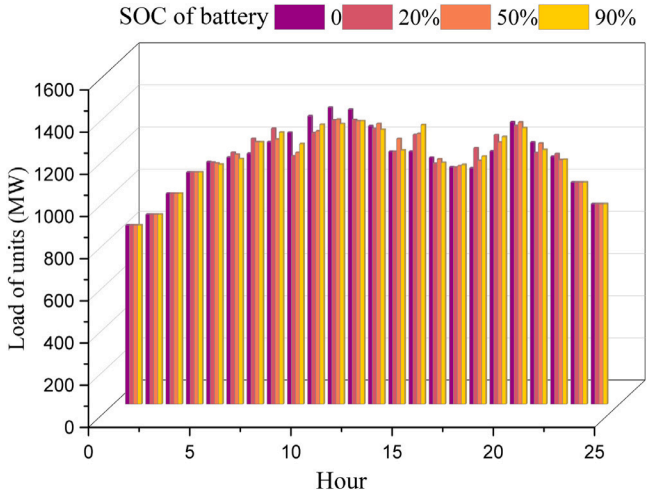


**Fig. 6.** The influence of various SOC of battery for UC problems.

to enhance the economic resilience of MESS, particularly in extreme operational conditions.

### 4.4. Benefit analysis for proposed MESSs

This section comprehensively studies the impact of photovoltaics and BESS as DGs, connected to the power grid load and integrated with PEVs to UC problem model, which will be divided into three cases to analyze and compare the effect of PEVs, DRGs on the grid system, and the benefits of MESSs for the grid system, the cases are shown in Table 5. And the photovoltaic data is experimented within 24 h of a day in Shenzhen in this research.

Fig. 6 shows the effect of different battery *SOC*s on unit load. It is not difficult seen that when the *SOC* of batteries is 90%, the load of units is lower than when the *SOC* is 0% in most time periods. This is because the battery can manage energy intelligently. When it is in a peak demand period, it can release the previously stored energy. At the same time, BESS can help reduce carbon emissions from electricity generated by fossil fuel. Therefore, the integration of PEVs and BESS is helpful to solve the high coupling UC problems.

The final optimal results of both DGs and PEVs integrated into UC problems are displayed in Table 7, Fig. 7 and Table 6 illustrates the comparison results of different UC problems in three cases. From

**Table 6**
Cost comparison for different cases.

| Case | Economic cost/($/day) | Difference | Carbon emission cost/($/day) | Difference |
|---|---|---|---|---|
| Case 1 | 651 393.15 | – | 656 881.77 | – |
| Case 2 | 641 151.03 | 1.57% | 640 398.12 | 2.51% |
| Case 3 | 638 540.54 | 1.97% | 638 998.57 | 2.72% |

Table 6, With respect to the economic cost consumed by unit operation, the fossil fuel cost and carbon emission cost of case 3 is 638540.54 $/day, which is 2610.49 $/day less than case 2 and 12852.61 $/day less than case 1. It is clear that the integration of PEVs and DGs can reduce the power generation cost and $CO_2$ emissions from the grid.

Fig. 7(b), shows the total power generated by 10 units per hour within 24 h, specifically in case 3, it can be evident that during the peak of demand at 12:00 am, the power generated by the unit is significantly lower compared to case 2 by 66.69 MW and case 1 by 102.34 MW, which validates that the integration of photovoltaics into the grid has a positive impact and saves power generation costs. Furthermore, it is observed that the overall trend of case3 is smoother than the other two cases, which effectively demonstrates that the integration of PEVs and DGs enhances the reliability of the electric grid system. According to Table 7, at 12:00am, the peak demand period, the discharge load of PEV is 78.7 MW lower than that in Table 2, indicating that the integration of DGs is also advantageous in managing the charge and discharge of PEVs. Compared with Tables 2 and 7, it is obvious that at 12:00, the generation capacity of the first 5 units in Table 2 exceeds 100 MW, and the generation capacity of the last 5 units is at least 10 MW, while only two units in Table 7 exceed 100 MW, which proves that DGs can mitigate the demand stress of the units and promote the reliability of the electrical grid under the premise of satisfying the demand.

No matter what the case is, the level-based learning method of BLLSO has a faster convergence speed and superior optimization results than other algorithms, as shown in Fig. 7(a). The comparative results between the original demand and the output power of thermal units in different cases is presented in Fig. 7(c), it is evident that case 3 has a larger gap between the two than cases 1 and 2, indicating that the proposed scheme can mitigate the demand pressure of traditional power generation in the grid, and at the same time mitigate the impact of climate change.

To summarize, the proposed binary LLSO is competitive and efficient when tackling strong coupling, high dimension and complicated UC problems. Moreover, the proposed system algorithm framework is conducive to the integration of PEVs charge and discharge management and distributed energy storage systems into the power system, while overcoming intermittency challenges, reducing dependence on fossil fuels and maximizing renewable resource utilization.

### 4.5. The performance of LLSO algorithm for UC problems

In this section, the focus is on analyzing the effects of the LLSO algorithm in solving UC problems. According to formula (1), the carbon

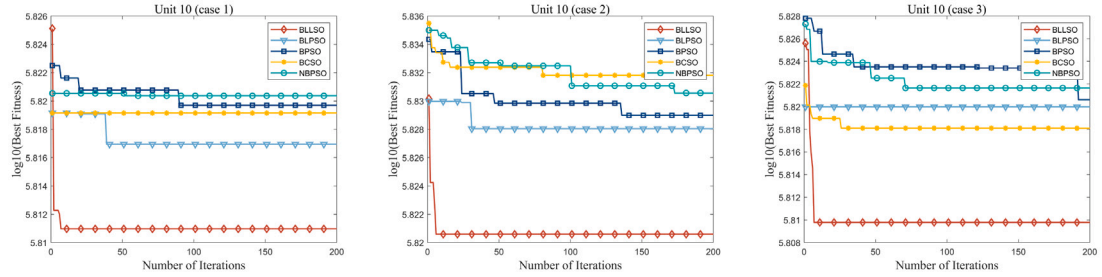


(a) Comparison of convergence curves in three cases.

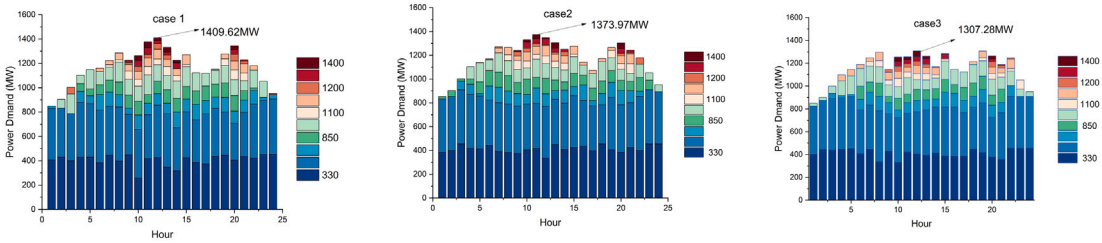


(b) Comparison of unit generation power in three cases.

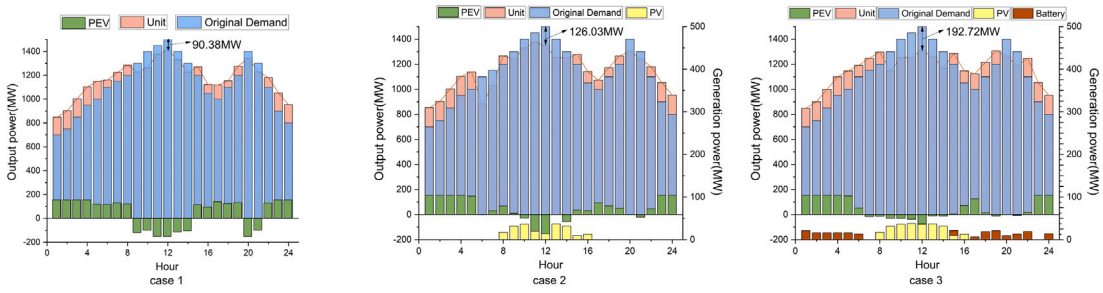


(c) Comparison of output power in three cases.

**Fig. 7.** Comparison of three analytical situations in three cases.

**Table 7**
The optimal results of UC integrated with PEVs and DGs.

| Hour | Unit1 (MW) | Unit2 (MW) | Unit3 (MW) | Unit4 (MW) | Unit5 (MW) | Unit6 (MW) | Unit7 (MW) | Unit8 (MW) | Unit9 (MW) | Unit10 (MW) | Demand (MW) | PEV Load (MW) |
|---|---|---|---|---|---|---|---|---|---|---|---|---|
| 1 | 401.18 | 422.59 | 0.00 | 0.00 | 25.00 | 0.00 | 0.00 | 0.00 | 0.00 | 0.00 | 700.00 | 153.00 |
| 2 | 442.94 | 431.85 | 0.00 | 0.00 | 25.00 | 0.00 | 0.00 | 0.00 | 0.00 | 0.00 | 750.00 | 153.00 |
| 3 | 439.50 | 451.08 | 45.64 | 0.00 | 63.55 | 0.00 | 0.00 | 0.00 | 0.00 | 0.00 | 850.00 | 153.00 |
| 4 | 445.14 | 451.45 | 20.00 | 0.00 | 130.57 | 0.00 | 52.11 | 0.00 | 0.00 | 0.00 | 950.00 | 153.00 |
| 5 | 452.15 | 455.00 | 20.00 | 0.00 | 162.00 | 0.00 | 57.08 | 0.00 | 0.00 | 0.00 | 1000.00 | 148.73 |
| 6 | 407.40 | 383.61 | 91.29 | 116.78 | 154.74 | 0.00 | 36.30 | 0.00 | 0.00 | 0.00 | 1100.00 | 51.41 |
| 7 | 444.90 | 387.80 | 113.31 | 88.91 | 139.72 | 39.66 | 33.13 | 0.00 | 0.00 | 0.00 | 1150.00 | −16.71 |
| 8 | 336.74 | 446.93 | 125.74 | 115.96 | 142.38 | 55.60 | 73.34 | 0.00 | 0.00 | 0.00 | 1200.00 | −13.15 |
| 9 | 427.39 | 330.17 | 96.19 | 56.35 | 99.40 | 43.85 | 66.73 | 26.39 | 0.00 | 0.00 | 1300.00 | −30.36 |
| 10 | 331.40 | 393.50 | 65.81 | 104.20 | 101.61 | 69.40 | 63.02 | 43.38 | 37.60 | 43.92 | 1400.00 | −30.82 |
| 11 | 421.24 | 339.97 | 92.68 | 75.62 | 143.96 | 49.51 | 41.71 | 29.43 | 32.04 | 29.54 | 1450.00 | −37.33 |
| 12 | 404.70 | 370.40 | 97.23 | 98.97 | 85.30 | 51.31 | 72.94 | 35.81 | 38.27 | 52.35 | 1500.00 | −74.30 |
| 13 | 391.95 | 399.55 | 86.99 | 88.98 | 86.37 | 54.33 | 53.99 | 28.12 | 46.38 | 25.47 | 1400.00 | −10.55 |
| 14 | 412.15 | 403.79 | 69.86 | 93.03 | 90.95 | 29.03 | 60.83 | 10.00 | 0.00 | 0.00 | 1300.00 | −11.13 |
| 15 | 387.85 | 428.51 | 130.00 | 111.23 | 160.56 | 20.00 | 0.00 | 0.00 | 37.50 | 10.00 | 1200.00 | 5.92 |
| 16 | 384.47 | 430.64 | 121.38 | 77.76 | 132.45 | 0.00 | 0.00 | 0.00 | 0.00 | 0.00 | 1050.00 | 73.36 |
| 17 | 386.85 | 380.06 | 107.90 | 113.55 | 135.60 | 0.00 | 0.00 | 0.00 | 0.00 | 0.00 | 1000.00 | 126.30 |
| 18 | 447.66 | 366.10 | 96.57 | 117.01 | 162.00 | 0.00 | 25.00 | 0.00 | 0.00 | 0.00 | 1100.00 | 14.44 |
| 19 | 416.93 | 434.43 | 119.26 | 115.98 | 134.40 | 26.94 | 58.34 | 0.00 | 0.00 | 0.00 | 1200.00 | −10.73 |
| 20 | 376.49 | 349.56 | 105.55 | 89.87 | 139.69 | 48.18 | 56.37 | 46.65 | 20.55 | 31.37 | 1400.00 | −0.45 |
| 21 | 356.72 | 408.68 | 90.08 | 117.74 | 106.24 | 35.39 | 43.37 | 19.29 | 10.59 | 0.00 | 1300.00 | −7.10 |
| 22 | 455.00 | 454.34 | 94.48 | 0.00 | 127.91 | 20.00 | 85.00 | 10.00 | 0.00 | 0.00 | 1100.00 | 18.72 |
| 23 | 455.00 | 455.00 | 0.00 | 0.00 | 63.00 | 80.00 | 0.00 | 0.00 | 0.00 | 0.00 | 900.00 | 153.00 |
| 24 | 455.00 | 454.74 | 0.00 | 0.00 | 40.54 | 0.00 | 0.00 | 0.00 | 0.00 | 0.00 | 800.00 | 153.00 |

emissions of PEVs and the cost of energy storage batteries are embedded in the objective function, which means the optimization goal is not only related to the UC problem. Therefore, to validate the effectiveness of the LLSO algorithm more accurately, the objective function should

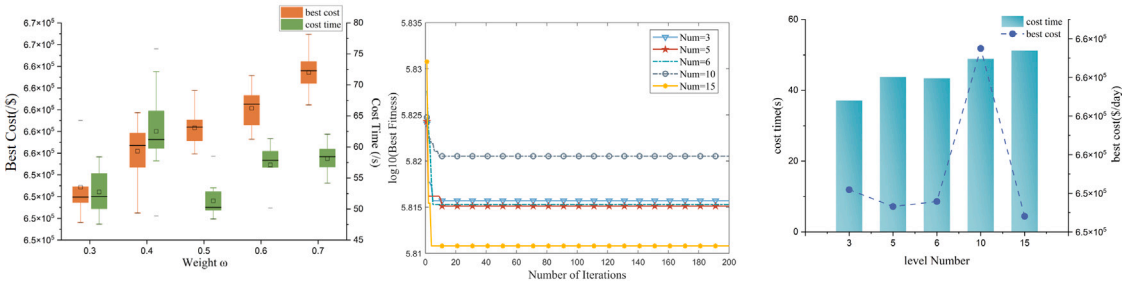


(a) The influence of different levels on the optimization results (b) The influence of different levels on convergence results (c) Compare results of different weights for the objective function

**Fig. 8.** Simulation results of different level numbers for the proposed LLSO.

**Table 8**
The comparison of economic costs between BLLSO and other algorithms ($/day).

| Methods / Units | BLLSO | BPSO | BLPSO | BCSO | NBPSO |
|---|---|---|---|---|---|
| 10 | **641151.03** | 660232.42 | 656059.77 | 659405.81 | 661257.79 |
| 20 | **1298683.07** | 1361712.85 | 1365531.02 | 1350198.56 | 1366159.31 |
| 40 | **2932930.70** | 3033901.32 | 3036362.36 | 3027874.59 | 3045861.33 |
| 60 | **5031276.71** | 5081598.26 | 5120236.23 | 5176234.85 | 5141295.51 |
| 80 | **7658985.91** | 7735412.70 | 7764308.78 | 7770574.64 | 7739865.17 |
| 100 | **10532931.32** | 10661547.12 | 10701986.46 | 10694520.02 | 10753241.4 |

be modified as below.

$$\begin{cases} F = \omega Cost + (1-\omega)\, Emission \\ Cost = min \sum_{t=1}^{T} \sum_{j=1}^{n} (F_j(P_{j,t}) z_{j,t} + SU_{j,t}(1 - z_{j,t-1}) z_{j,t}) \\ Emission = min \sum_{t=1}^{T} \sum_{j=1}^{n} F_j^{emi}(P_{j,t}) z_{j,t} \times pr_e \end{cases} \tag{23}$$

Eq. (23) is regarded as the optimization objective, the comparison experiments were conducted using four PSO variants, namely BLPSO, BPSO, NBPSO [19] and BCSO [53] to verify that the proposed optimization algorithm BLLSO can tackle the aforementioned problem. The economic cost optimization results of different algorithms and simulation curves in the evolution of different unit sizes are shown in Table 8 and Fig. 9. Before that, there are two parameters that need to be analyzed in detail because of their potential impact on the optimization results, which are the weight $\omega$ and the number of stratifications $L$. On the one hand, the weights in the objective function control the balance between generation costs and carbon emissions, so it is possible that different weighting factors may lead to different optimization results. On the other hand, different number of levels will lead to two consequences: if the number of $L$ is small, it means that each level contains more particles, which is beneficial to promote diversity in selecting higher level particles for learning. At the same time, the diversity in the selection levels is reduced because the quantity of levels is small. Conversely, a higher number of $L$ causes an increase in the diversity of level and a decrease in the diversity of selecting higher level particles.

Considering the above, the quantity of levels may have different effects on the evolutionary process. The simulation results of different weights and level numbers under 10-units benchmark problems are demonstrated in Fig. 8, which can be observed that different levels yield different results for the optimization results. Fig. 8(a) shows that the economic optimization value becomes higher as the weights increase, but the calculation cost is not the same. The difference in computational cost between weights 0.3 and 0.5 is smaller than other weight values, nevertheless, when the weight is 0.5, the economic cost optimization is larger than 0.3. Therefore, the weight is set to 0.3 can make a good compromise between economic cost and computational cost. When $L$ is 10, from Fig. 8(b) and Fig. 8(c) it can be observed that the optimization results and convergence speed are not as good as those less than 10. However, when the number of levels is 15, the optimization quality and convergence speed are obviously improved. Therefore, determining a reasonable number of levels plays a certain role in balancing exploration and exploitation.

Then, from Table 8, the economic costs optimized by different algorithms on the UC problem are compared for the number of units at 10, 20, 40, 60, 80 and 100, respectively. It is easy to see that the economic cost obtained by the BLLSO algorithm is always optimal compared to other algorithms, regardless of the quantity of units. In addition, the dimension of the UC problems is determined by the quantity of units, when the quantity of units is 10, the dimension of the UC problems is 10 (unit) × 24 (h) = 240. The minimum gap between the economic costs obtained from BLLSO and other algorithms is 14908.74 $/day, and the maximum gap reaches 220310.1 $/day when the quantity of units increases to 100. This proves that the BLLSO algorithm has a good potential competitiveness for solving large-scale, high-dimensional UC problems. Furthermore, from Fig. 9, the BLLSO algorithm clearly outperforms other algorithms in terms of convergence speed and optimization quality. This is due to the fact that the level-based learning strategy of BLLSO can improve the diversity, thereby mitigating the risks of convergence prematurely and stagnancy. When the quantity of units increases to 100, the BLLSO still outperforms other algorithms with regard to convergence speed and optimization quality. Overall, it can be seen that LLSO not only achieves a favorable equilibrium between exploration and exploitation abilities, but is also suitable for large scale optimization scenarios.

## 5. Conclusion

The integration of plug-in electric vehicles, photovoltaics, and battery energy storage systems into the power system offers multiple benefits, including grid stability, peak load management, renewable energy integration, and optimization of grid infrastructure, generating a large-scale optimization problem. In this paper, a multi-energy synergy system scheduling framework is proposed for the problem formulation. Further, a large-scale binary level-based learning swarm optimizer is proposed for generating units, taking into account the characteristics of the unit switching state, with the cost of fossil fuel and carbon emission optimized as objective functions. In this system framework, the binary level-based learning swarm optimization algorithm is adopted to

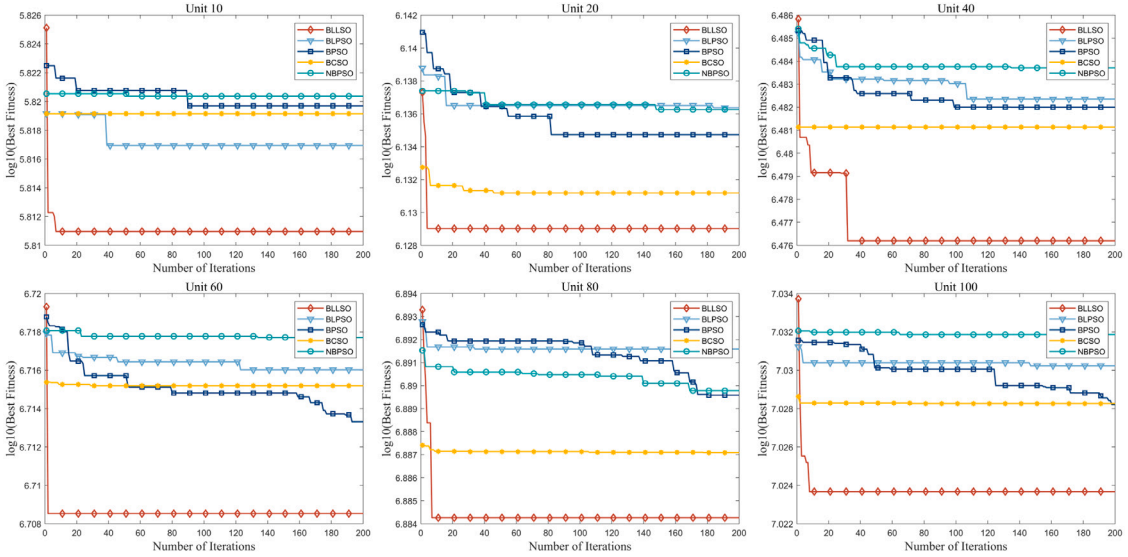


**Fig. 9.** Convergence curves of different algorithms with different unit numbers.

optimize the impact of integrating plug-in electric vehicle charge and discharge management, energy storage batteries, and photovoltaic into the grid.

To confirm the feasibility and necessity of the proposed scheme, three scenarios are discussed and their economic benefits to the grid are analyzed. The results of the experimental analysis demonstrate that the proposed algorithm is capable of attaining a cost reduction of more than 3.3%, which can reflect a highly competitive ability for solving complex high-dimensional energy systems. Therefore, the charge and discharge management of plug-in electric vehicles and distributed energy storage integration is of great importance in future power systems, with its low carbon emissions and renewable nature, which can bring economic benefits, as well as promoting the popularization of renewable energy and the transformation of the multi-energy synergy systems.

## CRediT authorship contribution statement

**Linxin Zhang:** Conceptualization, Data curation, Formal analysis, Methodology, Software, Visualization, Writing – original draft, Writing – review & editing. **Zhile Yang:** Conceptualization, Funding acquisition, Methodology, Project administration, Resources, Supervision, Validation, Writing – review & editing. **Qinge Xiao:** Conceptualization, Methodology, Project administration, Resources, Validation, Writing – review & editing. **Yuanjun Guo:** Conceptualization, Funding acquisition, Methodology, Project administration, Resources, Supervision, Validation, Writing – review & editing. **Zuobin Ying:** Conceptualization, Funding acquisition, Project administration, Resources, Supervision, Validation, Writing – review & editing. **Tianyu Hu:** Conceptualization, Data curation, Methodology, Software, Validation, Writing – review & editing. **Xiandong Xu:** Conceptualization, Project administration, Resources, Supervision, Validation, Writing – review & editing. **Sohail Khan:** Conceptualization, Project administration, Resources, Supervision, Validation, Writing – review & editing. **Kang Li:** Conceptualization, Project administration, Resources, Supervision, Validation, Writing – review & editing.

## Declaration of competing interest

We declare that we have no financial and personal relationships with other people or organizations that can inappropriately influence our work. There is no professional or other personal interest of any nature or kind in any product, service and/or company that could be construed as influencing the position presented in, or the review of, the manuscript.

## Data availability

The data that has been used is confidential.

## Acknowledgments

This research is financially supported by National Natural Science Foundation of China under grants 52077213 and 62003332, and Youth Innovation Promotion Association CAS 2021358, and Shenzhen Science and Technology Research and Development Fund JCYJ20200109114839874, and NSFC-FDCT under its Joint Scientific Research Project Fund (Grant No. 0051/2022/AFJ), China & Macau.

## References

[1] Liu Z, Sun Y, Xing C, Liu J, He Y, Zhou Y, et al. Artificial intelligence powered large-scale renewable integrations in multi-energy systems for carbon neutrality transition: Challenges and future perspectives. Energy AI 2022;100195.
[2] Yang S, Gao HO, You F. Integrated optimization in operations control and systems design for carbon emission reduction in building electrification with distributed energy resources. Adv Appl Energy 2023;100144.
[3] Sharma H, Marinovici L, Adetola V, Schaef HT. Data-driven modeling of power generation for a coal power plant under cycling. Energy AI 2023;11:100214.
[4] Yang W, Guo J, Vartosh A. Optimal economic-emission planning of multi-energy systems integrated electric vehicles with modified group search optimization. Appl Energy 2022;311:118634.
[5] Turk A, Wu Q, Zhang M, Østergaard J. Day-ahead stochastic scheduling of integrated multi-energy system for flexibility synergy and uncertainty balancing. Energy 2020;196:117130.
[6] Liu X, Yan Z, Wu J. Optimal coordinated operation of a multi-energy community considering interactions between energy storage and conversion devices. Appl Energy 2019;248:256–73.
[7] Shahbakhsh A, Nieße A. Modeling multimodal energy systems. Automatisierungstechnik 2019;67(11):893–903.
[8] Yang Z, Li K, Guo Y, Feng S, Niu Q, Xue Y, et al. A binary symmetric based hybrid meta-heuristic method for solving mixed integer unit commitment problem integrating with significant plug-in electric vehicles. Energy 2019;170:889–905.
[9] Zou W, Sun Y, Gao D-c, Zhang X, Liu J. A review on integration of surging plug-in electric vehicles charging in energy-flexible buildings: Impacts analysis, collaborative management technologies, and future perspective. Appl Energy 2023;331:120393.
[10] Zhang H, Moura SJ, Hu Z, Qi W, Song Y. Joint PEV charging network and distributed PV generation planning based on accelerated generalized benders decomposition. IEEE Trans Transp Electr 2018;4(3):789–803.
[11] Lander L, Kallitsis E, Hales A, Edge JS, Korre A, Offer G. Cost and carbon footprint reduction of electric vehicle lithium-ion batteries through efficient thermal management. Appl Energy 2021;289:116737.
[12] Lagos DT, Hatziargyriou ND. Data-driven frequency dynamic unit commitment for island systems with high RES penetration. IEEE Trans Power Syst 2021;36(5):4699–711.

[13] Kermani M, Shirdare E, Parise G, Bongiorno M, Martirano L. A comprehensive technoeconomic solution for demand control in ports: Energy storage systems integration. IEEE Trans Ind Appl 2022;58(2):1592–601.
[14] Zsiborács H, Pintér G, Vincze A, Baranyai NH, Mayer MJ. The reliability of photovoltaic power generation scheduling in seventeen European countries. Energy Convers Manage 2022;260:115641.
[15] Furukakoi M, Adewuyi OB, Matayoshi H, Howlader AM, Senjyu T. Multi objective unit commitment with voltage stability and PV uncertainty. Appl Energy 2018;228:618–23.
[16] Saber AY, Venayagamoorthy GK. Plug-in vehicles and renewable energy sources for cost and emission reductions. IEEE Trans Ind Electron 2011;58(4):1229–38.
[17] Joos M, Staffell I. Short-term integration costs of variable renewable energy: Wind curtailment and balancing in Britain and Germany. Renew Sustain Energy Rev 2018;86:45–65.
[18] Yang Z, Yang F, Min H, Tian H, Hu W, Liu J, et al. Energy management programming to reduce distribution network operating costs in the presence of electric vehicles and renewable energy sources. Energy 2023;263:125695.
[19] Yang Z, Li K, Niu Q, Xue Y. A novel parallel-series hybrid meta-heuristic method for solving a hybrid unit commitment problem. Knowl-Based Syst 2017;134:13–30.
[20] Boretti A. Integration of solar thermal and photovoltaic, wind, and battery energy storage through AI in NEOM city. Energy AI 2021;3:100038.
[21] Yildiz B, Stringer N, Klymenko T, Samhan MS, Abramowitz G, Bruce A, et al. Real-world data analysis of distributed PV and battery energy storage system curtailment in low voltage networks. Renew Sustain Energy Rev 2023;186:113696.
[22] Zeraati M, Golshan MEH, Guerrero JM. Distributed control of battery energy storage systems for voltage regulation in distribution networks with high PV penetration. IEEE Trans Smart Grid 2016;9(4):3582–93.
[23] Fleer J, Stenzel P. Impact analysis of different operation strategies for battery energy storage systems providing primary control reserve. J Energy Storage 2016;8:320–38.
[24] Guzmán-Feria JS, Castro LM, Tovar-Hernández J, González-Cabrera N, Gutiérrez-Alcaraz G. Unit commitment for multi-terminal VSC-connected AC systems including BESS facilities with energy time-shifting strategy. Int J Electr Power Energy Syst 2022;134:107367.
[25] Huang P, Sun Y, Lovati M, Zhang X. Solar-photovoltaic-power-sharing-based design optimization of distributed energy storage systems for performance improvements. Energy 2021;222:119931.
[26] Nishanthy J, Raja SC, Nesamalar JJD. Feasibility analysis of solar PV system in presence of EV charging with transactive energy management for a community-based residential system. Energy Convers Manage 2023;288:117125.
[27] Li Y, Wang P, Gooi HB, Ye J, Wu L. Multi-objective optimal dispatch of microgrid under uncertainties via interval optimization. IEEE Trans Smart Grid 2019;10(2):2046–58.
[28] Neri A, Butturi MA, Lolli F, Gamberini R. Inter-firm exchanges, distributed renewable energy generation, and battery energy storage system integration via microgrids for energy symbiosis. J Clean Prod 2023;414:137529.
[29] Su W, Chow M-Y. Computational intelligence-based energy management for a large-scale PHEV/PEV enabled municipal parking deck. Appl Energy 2012;96:171–82.
[30] Borozan S, Giannelos S, Strbac G. Strategic network expansion planning with electric vehicle smart charging concepts as investment options. Adv Appl Energy 2022;5:100077.
[31] Naderipour A, Kamyab H, Klemeš JJ, Ebrahimi R, Chelliapan S, Nowdeh SA, et al. Optimal design of hybrid grid-connected photovoltaic/wind/battery sustainable energy system improving reliability, cost and emission. Energy 2022;257:124679.
[32] Gomes I, Melicio R, Mendes V. A novel microgrid support management system based on stochastic mixed-integer linear programming. Energy 2021;223:120030.
[33] Colonetti B, Finardi E, Brito S, Zavala V. Parallel dual dynamic integer programming for large-scale hydrothermal unit-commitment. IEEE Trans Power Syst 2022;38(3):2926–38.
[34] Jiang Q, Zhou B, Zhang M. Parallel augment Lagrangian relaxation method for transient stability constrained unit commitment. IEEE Trans Power Syst 2013;28(2):1140–8.
[35] Feng F, Zhang P, Bragin MA, Zhou Y. Novel resolution of unit commitment problems through quantum surrogate Lagrangian relaxation. IEEE Trans Power Syst 2022.
[36] Arroyo JM, Conejo AJ. A parallel repair genetic algorithm to solve the unit commitment problem. IEEE Trans Power Syst 2002;17(4):1216–24.
[37] Trivedi A, Srinivasan D, Biswas S, Reindl T. A genetic algorithm–differential evolution based hybrid framework: case study on unit commitment scheduling problem. Inform Sci 2016;354:275–300.
[38] Simon SP, Padhy NP, Anand RS. An ant colony system approach for unit commitment problem. Int J Electr Power Energy Syst 2006;28(5):315–23.
[39] Ting T, Rao M, Loo C. A novel approach for unit commitment problem via an effective hybrid particle swarm optimization. IEEE Trans Power Syst 2006;21(1):411–8.
[40] Hussein BM, Jaber AS. Unit commitment based on modified firefly algorithm. Meas Control 2020;53(3–4):320–7.
[41] Roy PK, Sarkar R. Solution of unit commitment problem using quasi-oppositional teaching learning based algorithm. Int J Electr Power Energy Syst 2014;60:96–106.
[42] Yuan X, Su A, Nie H, Yuan Y, Wang L. Application of enhanced discrete differential evolution approach to unit commitment problem. Energy Convers Manage 2009;50(9):2449–56.
[43] Hussien AG, Hassanien AE, Houssein EH, Amin M, Azar AT. New binary whale optimization algorithm for discrete optimization problems. Eng Optim 2020;52(6):945–59.
[44] Pan J-S, Hu P, Chu S-C. Binary fish migration optimization for solving unit commitment. Energy 2021;226:120329.
[45] Kashan MH, Nahavandi N, Kashan AH. DisABC: a new artificial bee colony algorithm for binary optimization. Appl Soft Comput 2012;12(1):342–52.
[46] Lau T, Chung C, Wong K, Chung T, Ho SL. Quantum-inspired evolutionary algorithm approach for unit commitment. IEEE Trans Power Syst 2009;24(3):1503–12.
[47] Rizk-Allah RM. A quantum-based sine cosine algorithm for solving general systems of nonlinear equations. Artif Intell Rev 2021;54(5):3939–90.
[48] Wang F, Zhang H, Zhou A. A particle swarm optimization algorithm for mixed-variable optimization problems. Swarm Evol Comput 2021;60:100808.
[49] Cheng R, Sun C, Jin Y. A multi-swarm evolutionary framework based on a feedback mechanism. In: 2013 IEEE congress on evolutionary computation. IEEE; 2013, p. 718–24.
[50] Wang X, Henshaw P, Ting DS-K. Exergoeconomic analysis for a thermoelectric generator using mutation particle swarm optimization (m-PSO). Appl Energy 2021;294:116952.
[51] Cheng R, Jin Y. A social learning particle swarm optimization algorithm for scalable optimization. Inform Sci 2015;291(C):43–60.
[52] Wang X, Zhang K, Wang J, Jin Y. An enhanced competitive swarm optimizer with strongly convex sparse operator for large-scale multiobjective optimization. IEEE Trans Evol Comput 2021;26(5):859–71.
[53] Wang Y, Yang Z, Mourshed M, Guo Y, Niu Q, Zhu X. Demand side management of plug-in electric vehicles and coordinated unit commitment: A novel parallel competitive swarm optimization method. Energy Convers Manage 2019;196:935–49.
[54] Zhu X, Zhao S, Yang Z, Zhang N, Xu X. A parallel meta-heuristic method for solving large scale unit commitment considering the integration of new energy sectors. Energy 2022;238:121829.
[55] Feng L, Shang Q, Hou Y, Tan KC, Ong Y-S. Multispace evolutionary search for large-scale optimization with applications to recommender systems. IEEE Trans Artif Intell 2022;4(1):107–20.
[56] Li X, Lu S, Li Z, Wang Y, Zhu L. Modeling and optimization of bioethanol production planning under hybrid uncertainty: A heuristic multi-stage stochastic programming approach. Energy 2022;245:123285.
[57] Yang Q, Chen W-N, Da Deng J, Li Y, Gu T, Zhang J. A level-based learning swarm optimizer for large-scale optimization. IEEE Trans Evol Comput 2017;22(4):578–94.
[58] Zhang N, Hu Z, Dai D, Dang S, Yao M, Zhou Y. Unit commitment model in smart grid environment considering carbon emissions trading. IEEE Trans Smart Grid 2015;7(1):420–7.
[59] Lund H, Kempton W. Integration of renewable energy into the transport and electricity sectors through V2G. Energy Policy 2008;36(9):3578–87.
[60] Gaing Z-L. Discrete particle swarm optimization algorithm for unit commitment. In: 2003 IEEE power engineering society general meeting (IEEE cat. no. 03CH37491), vol. 1. IEEE; 2003, p. 418–24.
[61] Cheng R, Jin Y. A social learning particle swarm optimization algorithm for scalable optimization. Inform Sci 2015;291:43–60.
[62] Cheng R, Jin Y. A competitive swarm optimizer for large scale optimization. IEEE Trans Cybern 2014;45(2):191–204.
[63] Kazarlis SA, Bakirtzis AG, Petridis V. A genetic algorithm solution to the unit commitment problem. IEEE Trans Power Syst 1996;11(1):83–92.
[64] Zhao S, Li K, Yang Z, Xu X, Zhang N. A new power system active rescheduling method considering the dispatchable plug-in electric vehicles and intermittent renewable energies. Appl Energy 2022;314:118715.
[65] Xing C, Li K, Su J. Thermal constrained energy optimization of railway co-phase systems with ESS integration-an FRA-pruned DQN approach. IEEE Trans Transp Electr 2022.
[66] Quan H, Srinivasan D, Khambadkone AM, Khosravi A. A computational framework for uncertainty integration in stochastic unit commitment with intermittent renewable energy sources. Appl Energy 2015;152:71–82.